STAR FORMATION THRESHOLDS AND GALAXY EDGES: WHY AND WHERE

JOOP SCHAYE

School of Natural Sciences, Institute for Advanced Study, Einstein Drive, Princeton NJ 08540, schaye@ias.edu
Accepted for publication in the Astrophysical Journal

ABSTRACT

We study global star formation thresholds in the outer parts of galaxies by investigating the stability of disk galaxies embedded in dark halos. The disks are self-gravitating, contain metals and dust, and are exposed to UV radiation. We find that the critical surface density for the existence of a cold interstellar phase depends only weakly on the parameters of the model and coincides with the empirically derived surface density threshold for star formation. Furthermore, it is shown that the drop in the thermal velocity dispersion associated with the transition from the warm to the cold gas phase triggers gravitational instability on a wide range of scales. The presence of strong turbulence does not undermine this conclusion if the disk is self-gravitating. Models based on the hypothesis that the onset of thermal instability determines the star formation threshold in the outer parts of galaxies can reproduce many observations, including the threshold radii, column densities, and the sizes of stellar disks as a function of disk scale length and mass. Finally, prescriptions are given for implementing star formation thresholds in (semi-)analytic models and three-dimensional hydrodynamical simulations of galaxy formation.

Subject headings: galaxies: evolution — galaxies: formation — galaxies: ISM — ISM: clouds — stars: formation

1. INTRODUCTION

Observations of the distribution of Hα emission in disk galaxies show that the (azimuthally averaged) star formation rate (SFR) drops abruptly at a few disk scale lengths (e.g., Kennicutt 1989, hereafter K89; Martin & Kennicutt 2001, hereafter MK01). The fact that the gas disk typically extends far beyond this radius, suggests that the radial truncation of the SFR is due to a star formation threshold. If the truncation radius does not decrease with time and if stars remain at fixed radii after their formation, then one would also expect a sharp cutoff in the stellar surface density. There is evidence that stellar disks in galaxies are finite: the surface brightness distribution of spiral galaxies is observed to cut off beyond a few disk scale lengths (van der Kruit 1979; van der Kruit & Searle 1981). There are some indications that the two disk edges do coincide (e.g., van der Kruit 1988; K89), but the issue has yet to be investigated conclusively.

The existence of a surface density threshold for star formation is usually explained in terms of the Toomre criterion for gravitational instability (Spitzer 1968; Quirk 1972; Fall & Efstathiou 1980; K89). Neither rotation nor pressure can stabilize a thin, gaseous, differentially rotating disk if the Toomre Q parameter,

$$Q(r) \equiv \frac{c_s \kappa}{\pi G \Sigma_g},\qquad(1)$$

is less than unity (Safronov 1960; Toomre 1964; Goldreich & Lynden-Bell 1965; Binney & Tremaine 1987); where the effective sound speed c_s, the epicyclic frequency κ, and the gas surface density Σ_g all depend on radius r. K89 tested the hypothesis that the Toomre criterion is responsible for the observed cutoff in the SFR by measuring the ratio $\alpha \equiv 1/Q$ of the gas surface density Σ_g to the critical surface density

$$\Sigma_c(r) \equiv \frac{c_s \kappa}{\pi G} \equiv \frac{\Sigma_g}{\alpha} \equiv Q \Sigma_g \qquad(2)$$

for a sample of 15 spiral galaxies. Assuming a constant velocity dispersion of 6 kms⁻¹, he found that $\alpha \equiv \Sigma_g/\Sigma_c \approx$

0.5[1] at the truncation radius. This result was recently confirmed by MK01 who found from a sample of 32 well-studied nearby spiral galaxies that $\alpha = 0.53 \pm 0.2$. However, Hunter, Elmegreen, & Baker (1998, hereafter HEB98) measured $\alpha \approx 0.25$ for a sample of irregulars.

In an important paper, Elmegreen & Parravano (1994) proposed that star formation requires only the coexistence of two thermal phases in pressure equilibrium and suggested that the fact that Q becomes high beyond the optical edge is partly coincidental. They argued that high values of the Q parameter prevent star formation indirectly by removing the ability of the gas to form the high pressure regions that are required for the existence of a multiphase interstellar medium (ISM). The need for a cool phase was also emphasized by Gerritsen & Icke (1997), HEB98, Hunter, Elmegreen, & van Woerden (2001), Billett, Hunter, & Elmegreen (2002), and Elmegreen (2002).

There has been little discussion in the literature on the appropriate value of the velocity dispersion σ (but see Ferguson et al. 1998), which is difficult to measure observationally and is usually assumed to be independent of radius. K89 and MK01 assumed a constant value of 6 kms⁻¹, while HEB98 used 9 kms⁻¹ for their sample of irregular galaxies. It is interesting to note that the difference in the assumed velocity dispersion can account for the discrepancy in α between spirals and irregulars found by HEB98. If HEB98 had assumed $\sigma = 6$ kms⁻¹, they would have measured $\alpha \approx 0.37$ instead of 0.25, which would have agreed with the result obtained by K89 and MK01 at the 0.8 σ level.

Since the cold phase has a temperature that is roughly

---

[1] The Toomre criterion for a gaseous disk depends on the sound speed. However, most studies use the 1-D velocity dispersion $\sigma = c_s/\sqrt{\gamma}$ instead, where γ is the ratio of specific heats. To correct for this, the values for α quoted from these papers (K89, MK01, and HEB98) have been multiplied by a factor $1/\sqrt{\gamma}$, assuming $\gamma = 5/3$ (which is incorrect if the gas is highly molecular or if the velocity dispersion is dominated by turbulence). In addition, the values quoted by K89 and HEB98 have been multiplied by a factor $\pi/3.36$ because they used the Toomre criterion for a stellar disk instead of that for a gaseous disk.

two orders of magnitudes lower than that of the warm phase ($T \sim 10^2$ K vs. 10^4 K), and thus a thermal velocity dispersion that is smaller by a factor 10, it seems reasonable to assume that the phase transition has important consequences for the stability of the disk. Indeed, the importance of cooling below 10^4 K to the instability of disks has been recognized in other contexts, such as the formation of the first objects from gas free of metals and dust (e.g., Corbelli & Salpeter 1995; Corbelli, Galli, & Palla 1997; Oh & Haiman 2002). However, since the presence of even modest amounts of dust enhances the formation rate of molecular hydrogen by orders of magnitude, the results of these studies are probably only valid for the first generation of stars.

Here we investigate the importance of the transition from the warm ($T \sim 10^4$ K) to the cold ($T \sim 10^2$ K) interstellar phase to the stability of disk galaxies using a model of a gaseous, exponential disk embedded in a dark halo. The disk is self-gravitating, contains metals and dust, and is illuminated by UV radiation. The main conclusions are that 1) The transition to the cold phase occurs at a surface density that agrees with the empirically derived threshold surface density for star formation (e.g., Skillman 1987), which supports the idea of Elmegreen & Parravano (1994) that the existence of a cold phase is critical for star formation; 2) The large decrease in the thermal velocity dispersion associated with the transition to the cold phase triggers gravitational instability on a large range of scales.

Because the gas is thermally unstable at intermediate temperatures (Field 1965) and because self-shielding from the photodissociating UV-radiation provides a positive feedback loop, the transition from the warm, atomic to the cold, molecular phase is fairly sudden. Assuming hydrostatic equilibrium (i.e., a self-gravitating disk), we find that the critical surface density is about $\Sigma_c \sim 3$–10 $M_\odot\,pc^{-2}$ ($N_{H,crit} \sim 3$–10×10^{20} cm^{-2}), which corresponds to a pressure $P/k \sim 10^2$–10^3 cm^{-3} K and a volume density $n_H \sim 10^{-2}$–10^{-1} cm^{-3}. The threshold surface density is insensitive to the exact values of model parameters such as the intensity of the UV radiation, the metallicity, the turbulent pressure, and the mass fraction in collisionless matter.

An important result obtained in this work is that the phase transition triggers gravitational instability even in the presence of relatively strong turbulence. The reason is that turbulent support increases the surface density required for the phase transition by about as much as it increases the velocity dispersion of the gas, thereby leaving the Q parameter *at the radius of the phase transition* nearly unchanged. Indeed, we find that the turbulent pressure needs to be more than 250 times greater than the thermal pressure to prevent the phase transition from triggering gravitational instability. For the atomic phase this would correspond to a line of sight velocity dispersion greater than $10(T/10^2\,K)^{0.5}$ km s^{-1}, which exceeds the values typical for the outer parts of disks (8 km s^{-1}; e.g., Lo, Sargent, & Young 1993; Meurer et al. 1996). In fact, there is little room for turbulence in the extended gas disks. If the gas is warm beyond the truncation radius, as predicted by our model, the thermal velocity dispersion can fully account for the observed H I line widths.

Although the hypothesis that the transition to the cold phase sets the global star formation threshold in the outer parts of galaxies is physically reasonable and, as we shall show, appears to be supported by observations, it is important to note that there are other mechanisms that can trigger the formation of unstable, cold clouds. For example, shocks from spiral density waves and swing-amplifier instabilities can locally convert an otherwise purely warm phase into a multiphase medium.[2] However, to prevent photoionization from keeping the gas warm, these regions would also need to have surface densities exceeding the threshold for the formation of a cold phase and the phase transition would still trigger instability on small scales.

This paper is organized as follows. Before discussing the model in detail in §3, we provide an intuitive derivation of the Toomre criterion in §2. In this section we also derive an equivalent instability criterion for the case when shear is more important than the Coriolis effect in limiting the growth of perturbations. Readers who want to get straight to the results can skip §2 and read only the first paragraph of §3. In §4 we explore the physical cause of the existence of a critical radius for gravitational instability. In §5 scaling relations are presented for the threshold surface density as a function of the metallicity, the intensity of the UV radiation, the fraction of the pressure that is non-thermal, and the fraction of the mass in gas. This section also contains recipes for implementing star formation thresholds in (semi-)analytic and numerical models of galaxy formation. In §6 we compare the model with observations and show that the predictions for the threshold column densities and radii agree with the data. Furthermore, it is shown that other predictions of the model, including a sharp drop in the molecular fraction, are also supported by observations. It is also demonstrated that the model correctly predicts the sizes of stellar disks and their variation with disk scale length and mass. Finally, §7 contains a summary of the main conclusions.

2. GRAVITATIONAL INSTABILITY IN A ROTATING DISK

Although there are multiple derivations of the Toomre criterion (e.g., Binney & Tremaine 1987) and the equivalent instability criterion for shearing perturbations (e.g., Elmegreen 1993) in the literature, I have been unable to find a previous derivation in terms of timescales. The derivations are included here for pedagogical reasons.

Gravitational instability of a fluid requires that the self-gravity of a perturbation exceeds its internal pressure. In terms of timescales, a perturbation is gravitationally unstable if the local dynamical timescale is smaller than the sound-crossing timescale across the perturbation (or, equivalently, if the size of the perturbation exceeds the local Jeans length).

The dynamical timescale for a perturbation of size λ and surface density Σ within a thin disk is

$$t_{\rm dyn} \equiv \sqrt{\frac{\lambda}{G\Sigma}} \sim \sqrt{\frac{\lambda}{a}}, \qquad (3)$$

where a is the gravitational acceleration. The sound crossing timescale is

$$t_{\rm sc} \equiv \frac{\lambda}{c_s}. \qquad (4)$$

Hence, stability against gravitational collapse requires

$$\lambda < \frac{c_s^2}{G\Sigma}. \qquad (5)$$

Pressure is not the only restoring force in a rotating disk. Unless the circular velocity relative to the center of the galaxy

---

[2] Note that *consequences* of star formation, such as expanding shells and turbulence generated by supernovae, should not be taken into account when computing a global star formation threshold even though they may be very important for star formation in a multiphase ISM.

scales as $v \propto r^{-1}$, conservation of angular momentum forces a perturbation to rotate around its own center, thereby providing centripetal support. The natural timescale for the internal rotation of the perturbation is the epicyclic period $2\pi/\kappa$, where κ is the epicycle frequency,

$$\kappa^2 = 2\left(\frac{v^2}{r^2} + \frac{v}{r}\frac{dv}{dr}\right). \tag{6}$$

The equation of motion for a circular orbit can be obtained by equating the dynamical timescale and the rotation period $t_{\rm rot}$, and the criterion for instability is $t_{\rm dyn} < t_{\rm rot}$. For the *internal* rotation of a perturbation in a rotating disk we have $t_{\rm rot} = 2\pi/\kappa$, and stability against gravitational collapse thus requires

$$\lambda > \frac{4\pi^2 G\Sigma}{\kappa^2} \equiv \lambda_{\rm crit}. \tag{7}$$

Equations (5) and (7) cannot both be satisfied if $c_s^2/G\Sigma < 4\pi^2 G\Sigma/\kappa^2$, i.e., if $c_s\kappa/2\pi G\Sigma < 1$. As expected, this agrees with the Toomre criterion, $Q < 1$, to within a dimensionless factor of order unity (two). It is important to note that $Q < 1$ does not imply instability to perturbations of arbitrary wavelengths. Equations (5) and (7) indicate that perturbations with $\lambda < c_s^2/G\Sigma$ are stabilized by pressure, while perturbations with $\lambda > \lambda_{\rm crit}$ are stabilized by rotation.

For a perturbation of length λ, the exact dispersion relation (see, e.g., equation [6-47] of Binney & Tremaine 1987) can be solved to give the critical value of Q, below which the perturbation is unstable[3],

$$Q_c(\lambda) = 2\sqrt{\frac{\lambda}{\lambda_{\rm crit}} - \left(\frac{\lambda}{\lambda_{\rm crit}}\right)^2}. \tag{8}$$

As before, perturbations with $\lambda > \lambda_{\rm crit}$ are always stable. For $\lambda \ll \lambda_{\rm crit}$ equation (5) is recovered exactly. Hence, for small wavelengths rotation is unimportant, and the Toomre criterion asymptotes to the two-dimensional Jeans criterion.

Besides forcing perturbations to rotate around their centers (the Coriolis effect), galactic rotation can prevent the collapse of perturbations through another mechanism: shear (e.g., Elmegreen 1993; HEB98). If the disk is in differential rotation, then perturbations will be unable to collapse unless the shearing timescale is longer than the dynamical timescale. The shear rate is given by Oort's constant A,

$$t_{\rm shr}^{-1} \sim |A| \equiv \frac{1}{2}r\left|\frac{d\Omega}{dr}\right| = \frac{1}{2}\left|\frac{v}{r} - \frac{dv}{dr}\right|. \tag{9}$$

Stability against gravitational collapse requires $t_{\rm shr} < t_{\rm dyn}$, i.e.,

$$\lambda > \frac{G\Sigma}{A^2}. \tag{10}$$

Equations (5) and (10) cannot both be satisfied if $Q_{\rm shr}$ is less than unity, where

$$Q_{\rm shr} \equiv \frac{c_s A}{G\Sigma}. \tag{11}$$

The "Q parameter" for shearing perturbations is identical to the Toomre parameter (equation 1), except that κ is replaced by πA. In particular, the critical surface density is again proportional to the velocity dispersion. The epicycle frequency is compared with the factor πA in Fig. 1 for two galaxy models (dot-dashed and dotted curves respectively).

------

[3] A similar result can be derived from the relation $1/t_{\rm dyn} = 1/t_{\rm sc} + 1/t_{\rm rot}$.

The rotation curves of galaxies are observed to be flat in the outer parts, i.e., $dv/dr \ll v/r$. In this limit $Q_{\rm shear} \to Q\pi/2\sqrt{2} \approx 1.11Q$. If the rotation curve is rising, then A can be much smaller than κ, indicating that the Coriolis effect is more important than shear for limiting the growth of perturbations. For all galaxy models tested, the difference between the two Q parameters at the transition to the cold phase turned out to be small compared to the drop in the velocity dispersion associated with this phase transition (see e.g. Fig. 2). Thus, the presence of shear does not change the conclusion that the phase transition causes instability. In the following we will therefore generally only consider the Toomre criterion, noting that using the shear criterion instead would yield nearly identical results.

3. MODEL

To investigate the stability of disk galaxies, the model of Mo, Mao, & White (1998, hereafter MMW98) for an exponential disk embedded in a dark halo, is combined with the photoionization package CLOUDY (Ferland et al. 1998), which includes most of the microphysics that is thought to be relevant for the ISM. For each radius CLOUDY is used to compute the equilibrium temperature and ionization balance for a range of densities, modeling the disk as a constant density photo-dissociating region. From this grid of models, we then pick the density for which the disk is in hydrostatic equilibrium. The methods used to compute the density profile and the thermal and ionization balance are discussed in detail in sections 3.1 and 3.2 respectively. The results depend on the metallicity Z, the UV radiation field I, and the dimensionless factor $f \equiv f_g/f_{th}$, where f_g is the fraction of the mass in gas and f_{th} is the ratio of the thermal pressure to the total pressure. We choose $Z = 0.1Z_\odot$, $I = 10^6$ hydrogen ionizing photons $\rm cm^{-2}\,s^{-1}$, and $f = 1$ as our fiducial parameters, a choice that is motivated in §3.3. In §5 we show how the results scale with these parameters. In §4 we illustrate the results using two galaxy models: models HSB and LSB have a mass M_{200} and a dimensionless spin parameter λ of $(10^{12}\,{\rm M_\odot}, 0.05)$ and $(5 \times 10^{10}\,{\rm M_\odot}, 0.1)$ respectively (see §3.1 for further details). The rotation curves for these models are shown in Figure 1.

The following cosmology will be adopted: total matter density $\Omega_m = 0.3$, vacuum energy density $\Omega_\Lambda = 0.7$, Hubble constant $H_0 = 100\,h\,{\rm km\,s^{-1}\,Mpc^{-1}}$, $h = 0.65$. The helium mass fraction is assumed to be $Y = 0.24$.

3.1. *Dynamics*

MMW98 provide an analytic model for a self-gravitating disk embedded in a dark halo based on the following assumptions: (1) the disk contains a fraction m_d of the total mass; (2) the disk contains a fraction j_d of the total angular momentum; (3) the disk is a thin, centrifugally supported structure with an exponential density profile; (4) the disk is embedded in a halo that initially had a NFW profile (Navarro, Frenk, & White 1997), but responded adiabatically to the assembly of the disk (remaining spherical while it contracted).

NFW found that the following density profile provides a good fit to the equilibrium density profiles of the cold dark matter (CDM) halos in their N-body simulations,

$$\frac{\rho(r)}{\rho_{\rm crit}} = \frac{\delta_c}{(r/r_s)(1+r/r_s)^2}, \tag{12}$$

where $\rho_{\rm crit} = 3H^2/8\pi G$ is the critical density, δ_c is a characteristic density, and r_s is a scale radius. Defining the virial radius

r_{200} as the radius within which the mean density is $200\rho_{\text{crit}}$, it can be shown that

$$\delta_c = \frac{200}{3} \frac{c^3}{\ln(1+c) - c/(1+c)}, \qquad (13)$$

where c the halo concentration factor,

$$c \equiv r_{200}/r_s. \qquad (14)$$

The NFW profile for the density distribution of a dark halo is specified by the redshift (which we will set to zero), the cosmological parameters $(\Omega_m, \Omega_\Lambda, H_0)$, the concentration factor c, and the mass M_{200} (defined as the mass interior to r_{200}).

The disk is assumed to have an exponential surface density profile,

$$\Sigma = \Sigma_0 \exp(-r/R_d), \qquad (15)$$

where $\Sigma_0 = m_d M_{200}/2\pi R_d^2$ and the disk scale length is given by

$$R_d = \frac{1}{\sqrt{2}} \left(\frac{j_d}{m_d} \right) \lambda r_{200} f_c(c)^{-1/2} f_R(\lambda, c, m_d, j_d), \qquad (16)$$

where f_c and f_R are dimensionless factors of order unity defined by equations (23) and (32) of MMW98, and λ is the dimensionless spin parameter of the halo,

$$\lambda \equiv J|E|^{1/2} G^{-1} M_{200}^{-5/2}, \qquad (17)$$

where E is the total energy of the halo. The rotation curve is computed assuming that the halo responds adiabatically to the slow assembly of the disk as described in §2.3 of MMW98. For a given redshift and cosmology, the MMW98 disk model can thus be fully specified by the parameters, c, m_d, j_d, λ, and M_{200}.

Most results will be presented for two model galaxies: a high and a low surface brightness galaxy (models HSB and LSB respectively). We set $z = 0$, $c = 10$, $m_d = 0.05$, and $j_d = m_d$ for both models; MMW98 demonstrate that models with these parameter values (and distributions of λ and M_{200} that fit CDM simulations) agree with the observed Tully-Fisher relation (but see Borriello & Salucci 2001). Models with $c \sim 10$ also provide good fits to the observed rotation curves of dwarf galaxies (van den Bosch & Swaters 2001). Model HSB has $M_{200} = 10^{12}$ M$_\odot$ ($v_{200} \approx 141$ km s^{-1}) and $\lambda = 0.05$, while model LSB has $M_{200} = 5 \times 10^{10}$ M$_\odot$ ($v_{200} \approx 52$ km s^{-1}) and $\lambda = 0.1$. Hence, the disk scale length is 4.7 kpc for model HSB and 3.9 kpc for model LSB. The rotation curves for models HSB and LSB are shown in Figure 1. The maximum circular velocity is 218 km s^{-1} for model HSB and 72 km s^{-1} for model LSB. Figure 1 (*dot-dashed curves*) shows the epicycle frequency. With this choice of parameters models HSB and LSB are typical high and low surface brightness galaxies in terms of their surface density profiles and rotation curves. We have searched parameter space and checked that none of our conclusions are specific to these particular models.

The disk is illuminated by an external radiation field. To compute the thermal and ionization structure numerically, we need to specify the full density profile $\rho(r,z)$. For an isothermal, exponential disk, this distribution has been computed by Spitzer (1942). However, since the radial variation in the temperature is one of the key ingredients of the present work, we cannot assume isothermality.

To simplify the numerics, the vertical density stratification is neglected in the radiative transfer calculation, i.e., we assume that the density varies smoothly with radius, but is a step function in the z-direction. This assumption is reasonable because the column density weighted density,

$$\langle \rho(r) \rangle_N \equiv \frac{1}{\Sigma(r)} \int \rho(r,z)^2 dz, \qquad (18)$$

which is the relevant density for the radiative transfer calculation, is close to the midplane density for realistic profiles. In other words, in the region that contributes significantly to the surface density, the density is of order the midplane density. For example, for an isothermal, exponential disk the midplane density is just 1.5 times the column density weighted density.

The density and the column density can be related using the following argument. In (local) hydrostatic equilibrium the thickness of the disk, i.e., the size of the region over which the density is of order the characteristic density, is of order the local Jeans length L_J. Thus, the column density is of order the 'Jeans column density' (see Schaye 2001a for a derivation),

$$N_{H,J} \equiv n_H L_J,$$
$$= \left(\frac{\gamma k}{\mu m_H^2 G} \right)^{1/2} (1-Y)^{1/2} f^{1/2} n_H^{1/2} T^{1/2},$$
$$\approx 3.06 \times 10^{21} \text{ cm}^{-2} \, \mu^{-1/2} f^{1/2} \left(\frac{n_H}{1 \text{ cm}^{-3}} \right)^{1/2} T_4^{1/2}, (19)$$

where γ is the ratio of specific heats, μ is the mean particle weight in units of the hydrogen mass m_H, n_H is the hydrogen number density, $T \equiv T_4 \times 10^4$ K, and $f \equiv f_g/f_{th}$ where f_g is the fraction of the mass in gas and f_{th} is the ratio of the thermal pressure to the total pressure. In the appendix it is demonstrated that for an isothermal, purely gaseous disk equation (19) agrees with the exact solution to within 2 percent.

The hydrogen column density can be converted into a total gas surface density using

$$\Sigma_g \approx 1.05 \, M_\odot \, \text{pc}^2 \left(\frac{N_H}{10^{20} \text{ cm}^{-2}} \right) \left(\frac{1-Y}{0.76} \right)^{-1}. \qquad (20)$$

For fixed f_g, there is a one-to-one relation between the total pressure and the total hydrogen column density:

$$P = \frac{n_H kT}{\mu(1-Y)f_{th}},$$
$$= \frac{m_H^2 G}{f_g \gamma (1-Y)^2} N_H^2,$$
$$\approx \frac{k}{f_g} \left(\frac{N_H}{2.67 \times 10^{19} \text{ cm}^{-2}} \right)^2 \text{ cm}^{-3} \text{ K}, \qquad (21)$$

where we used equation (19) to go from the first to the second equality. Hence, any critical column/surface density can be converted into an equivalent critical pressure.

Note that if a cold phase is present, the situation is likely more complicated than our model suggests. The presence of a cold phase leads to star formation and thus turbulence, and the amount of turbulent support may be different for the different phases. More importantly, feedback from star formation produces a third, hot phase and large variations in the local radiation field. The model used here ignores these and other complications and can therefore not reliably predict the structure of a multiphase ISM. What it can do, however, is predict what is relevant for the present study: the column density or, equivalently, the pressure at which the transition to the cold phase occurs.
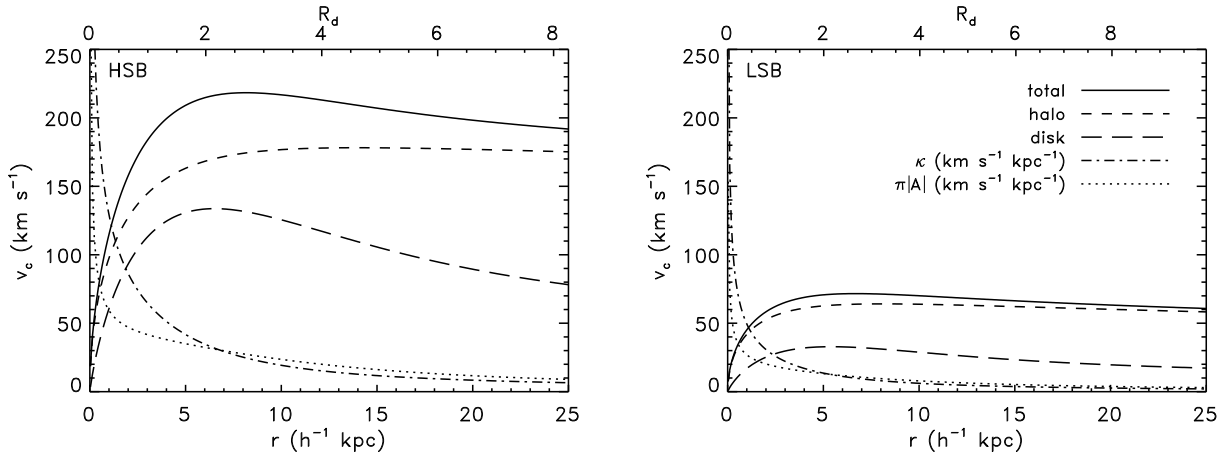
FIG. 1.— Circular velocity as a function of radius for models HSB (*left*) and LSB (*right*), showing the contributions of the halo (*short-dashed curves*) and those of the disk (*long-dashed curves*). Also shown are the epicycle frequency (*dot-dashed curves*) and π times Oort's constant A (*dotted curves*), both in $\mathrm{km\,s^{-1}\,kpc^{-1}}$.

3.2. *Thermal and ionization balance*

The thermal and ionization structure of the disk is computed using the publicly available photoionization package CLOUDY (version 94; Ferland et al. 1998, Ferland 2000), modeling the disk as a plane-parallel slab of constant density and assuming both thermal and ionization equilibrium. Illumination from two sides is approximated by doubling the column densities computed for a model illuminated from one side, which is reasonable if the disk is strongly self-shielded. The heating and cooling rates are computed self-consistently from the assumed incident continuum, which is described in §3.3.

For a given total hydrogen column density N_H, density n_H, incident radiation field I, metallicity Z, and dust-to-metals ratio, CLOUDY is used to compute the column densities in neutral hydrogen N_{HI} and molecular hydrogen N_{H_2}, the temperature T, and the mean particle mass μm_H (T and μ are first computed using a multi-zone model of a photo-dissociation region, but are then averaged over disk height z). CLOUDY contains nearly all microphysical processes that are thought to be relevant for the ISM and has been tested extensively on a wide variety of problems. The reader is referred to the online[4] documentation for details.

The disk model of MMW98 provides us with the surface density as a function of radius. Since we do not know a priori the density for which the disk is in hydrostatic equilibrium (i.e., eq. [19] is satisfied), we use the two-step procedure of Schaye (2001b) to compute the structure of the disk. First, CLOUDY is used to compute T and μ for a grid of (N_H, n_H) models. Second, for each radius (i.e., for each value of N_H) those solutions $(N_H, n_H, T(N_H, n_H), \mu(N_H, n_H))$ are selected for which equation (19) is satisfied and which are stable ($dP/dn_H > 0$). If there are two stable solutions for a fixed N_H, then the low temperature solution is selected because we are interested in the smallest column density for which the cold phase exists. Since the range of N_H for which two solutions are possible is small for all the models that were tested, picking the high temperature solution instead would not change the results significantly. Note that if N_H is large enough that only the low temperature solution is possible, this does not

mean that there is no warm phase, but merely that the fraction of gas in the warm phase, which always exists at sufficiently large scale heights, is small compared to that in the cold phase.

In summary, for each radius (i.e., surface density), we first compute the equilibrium temperature and ionization balance for a range of densities and then we pick the lowest temperature solution for which the disk is thermally stable and in hydrostatic equilibrium.

3.3. *Fiducial parameter values*

The parameters for the MMW98 disk model [$c = 10$, $m_d = 0.05$, $j_d = m_d$, $(M_{200}, \lambda)_{\mathrm{HSB}} = (10^{12}\,\mathrm{M_\odot}, 0.05)$, $(M_{200}, \lambda)_{\mathrm{LSB}} = (5 \times 10^{10}\,\mathrm{M_\odot}, 0.1)$] have already been discussed in §3.1. In this section we will motivate our fiducial values for the parameter f (recall that $f \equiv f_g/f_{th}$ where f_g is the fraction of the mass in gas and f_{th} is the ratio of the thermal pressure to the total pressure), the metallicity Z, the intensity of the UV radiation I, and the dust-to-metals ratio. In §5 we will see how the results change if different parameter values are used. Fortunately, the star formation threshold turns out to be insensitive to small (an order of magnitude or less) variations in these parameter values.

It is unclear how the factor f can be measured, but it seems reasonable to assume that $f \sim 1$ beyond the critical radius for star formation, since both the mass fraction in gas and the ratio of the thermal to total pressure are likely to be close to unity in the absence of star formation. For this reason we choose $f = 1$ as our fiducial value.

The metallicity is measurable, although measurements based on emission lines are generally only possible in regions of ongoing star formation, while absorption studies require the good fortune of a bright background source. Emission line studies of H II regions indicate that the metallicity is generally of order 10 percent solar near the optical edge (e.g., Ferguson et al. 1998a; Henry & Worthey 1999). Studies of damped Lyα absorption lines give similar values, although the scatter is large (e.g., Pettini et al. 1999). We will use $Z = 0.1\,Z_\odot$ as our fiducial value.

Comparisons of the relative abundance of refractory and non-refractory elements in damped Lyα systems indicate that the dust-to-metals ratio is about half that of the Galactic value (e.g., Pettini et al. 1997; Vladilo 1998), and we will therefore

---

[4] http://www.nublado.org.

use this as our fiducial value. The default dust composition of CLOUDY is used, i.e., a mixture of silicates and graphites with ISM properties. Depletion of metals onto dust grains is taken into account, using CLOUDY's default depletion factors.

The most uncertain parameter is undoubtedly the intensity of the UV radiation. Measurements of the present-day intensity of the extragalactic UV background provide a strong lower limit of $I \sim 10^{4.5}$ hydrogen ionizing photos $\mathrm{cm^{-2}\,s^{-1}}$ (ionization rate $\Gamma \sim 10^{-14}\ \mathrm{s^{-1}}$) with an uncertainty of a factor of a few (Scott et al. 2002 and references therein). However, the UV radiation illuminating the thick gas disk just beyond the critical radius is likely to be significantly more intense than this, and could well show strong spatial fluctuations. In addition to the extragalactic UV background (for which we assume the spectral shape of the model of Haardt & Madau 2001, which includes the extragalactic X-ray background, and the normalization of Scott et al. 2002), we use a component with the spectral shape of the unextinguished local interstellar radiation field of Black (1987) (using the CLOUDY command "table ISM") so that the total, i.e., extragalactic plus local, intensity of the UV radiation above 1 Rydberg is I photons $\mathrm{cm^{-2}\,s^{-1}}$. Finally, we add two more components: the cosmic microwave background and a cosmic ray density of $2 \times 10^{-9}\ \mathrm{cm^{-3}}$. However, the addition of these last two components does not have a significant effect on the star formation threshold.

The model of Bland-Hawthorn & Maloney (1999; 2002, see their Fig. 3) for the UV radiation field of the Galaxy, which includes contributions from the bulge, disk, halo, and the cosmic background, predicts an intensity of order $10^6\ \mathrm{ph\,cm^{-2}\,s^{-1}}$ at the truncation radius of the Galaxy (≈ 12 kpc, Freudenreich 1998), and we take this as our fiducial value. For LSB galaxies and H II regions beyond the critical radius a lower value may be more appropriate. In §5 it is shown that using just the extragalactic radiation field, reduces the critical surface density only by about a factor two.

Apart from the normalization, the shape of the spectrum also affects the surface density at which the phase transition takes place. A harder spectrum increases the heating rates, which increases the critical surface density. To test the sensitivity to the assumed spectral hardness, we computed a model using the spectral shape of the Haardt & Madau (2001) model for the extragalactic background (which has a softness parameter $S \equiv \Gamma_{\mathrm{HI}}/\Gamma_{\mathrm{HeII}} \approx 5.6 \times 10^2$, whereas the spectrum of Black 1987 has $S \approx 2.7 \times 10^3$) for the local UV radiation, leaving the normalization unchanged. Again, the difference in the critical surface density is only a factor of two.

4. THE PHYSICAL CAUSE OF STAR FORMATION THRESHOLDS

The solid curves in figure 2 show the Toomre Q parameter as a function of radius for models HSB (*left*) and LSB (*right*). At the critical radius r_c the Q parameters drop sharply from $Q > 2$ at $r > r_c$ to values smaller than unity at $r < r_c$ ($r_c \approx 4.3R_d$ for model HSB and $\approx 1.7R_d$ for model LSB). This sudden decrease is associated with a similar drop in the temperature (*dashed curves*) from $T \approx 10^4$ K to $< 10^3$ K and with a sharp increase in the molecular hydrogen fraction (the dot-dashed curves in figure 2 show $5 + \log f_{H_2}$) from $f_{H_2} \ll 10^{-3}$ to more than 10^{-3}.

As discussed in §2, besides the Coriolis effect, which the Toomre criterion takes into account, shear is another consequence of galactic rotation which can prevent the growth of perturbations. The dotted curves in figure 2 show that, as expected (see §2), the instability parameter for shearing perturbations, Q_{shr}, shows a similar behavior as the Toomre Q parameter, indicating that shear cannot stabilize the cold phase.

The fact that Q is significantly greater than unity for $r > r_c$ and then drops sharply to $Q < 1$ at $r \approx r_c$ implies that it is the transition to the cold phase that causes gravitational instability and not vice versa. Note that since both the surface density (Fig. 2, *triple-dot–dashed curves*) and the epicycle frequency (Fig. 1, *dot-dashed curves*) vary smoothly across r_c, it must be the decrease in the sound speed associated with the phase transition that causes the drop in Q.

As discussed in §2, $Q < 1$ only implies instability to perturbations of size $\lambda_{\mathrm{crit}}/2$, which is typically $\gtrsim$ kpc in the outer disk. Instability on smaller scales requires smaller values of Q (see eq. [8]). Figure 3 demonstrates that perturbations with $\lambda \ll \lambda_{\mathrm{crit}}$ do become unstable in the cold phase. The dash-dotted curves indicate the Q thresholds required for the instability of perturbations with wavelengths of (*top to bottom*) 10^3, 10^2, and 10 pc respectively. The sharpness of the drop in the Q value associated with the phase transition causes fluctuations of 1 kpc and 10^2 pc to become unstable at nearly the same surface density.

The transition to the cold phase coincides with a large increase in the molecular fraction. This is because the density, and thus the H_2 formation rate, must increase as the temperature decreases to prevent a drop in the internal pressure. Furthermore, the higher molecular fraction increases the cooling rate, providing a positive feedback loop. Other reasons why the transition to the cold phase is sudden are that the gas is thermally unstable at intermediate temperatures ($T \sim 10^3 - 10^4$ K) and that the increase in the molecular fraction enhances the self-shielding from photodissociating radiation, thereby providing another positive feedback loop.

After the phase transition the gas is gravitationally unstable and will fragment into clouds with a higher column density than the azimuthally averaged column density used in the models. This will make self-shielding more effective and will thus lead to a further decrease in the temperature and a further increase in the molecular fraction. This self-reinforcing process of cooling and collapse will not continue indefinitely, as the clouds will eventually become opaque to their own cooling radiation. Observations indicate that molecular clouds do form stars and it therefore seems plausible to associate the transition to the cold phase, which we have shown to trigger gravitational instability on a large range of scales, with the critical radius for star formation. In §6 we will show that the observations support this hypothesis.

Equation (19), which assumed local hydrostatic equilibrium, shows that if the temperature T, the mean molecular weight, and the factor f ($\equiv f_g/f_{th}$, where f_g is the fraction of the mass in gas and f_{th} is the ratio of the thermal to the total pressure) are constant, as is roughly the case beyond the critical radius where only the warm phase is present, then there is a one to one relation between density and column density or, equivalently, pressure. For fixed T, f, metallicity Z, and UV radiation field I, the existence of a cold phase depends on the density and the column density. Because the latter two are related one-to-one, the phase transition occurs at a fixed surface density ($\log N_{H,\mathrm{crit}} \approx 20.75$ for our fiducial parameters). Hence, there exists a threshold surface density for star formation, which does not depend on the rotation curve of the galaxy. The difference in the critical radii between the two models can therefore be explained in terms of their surface density profiles (Fig. 2, *triple-dot–dashed curves*).
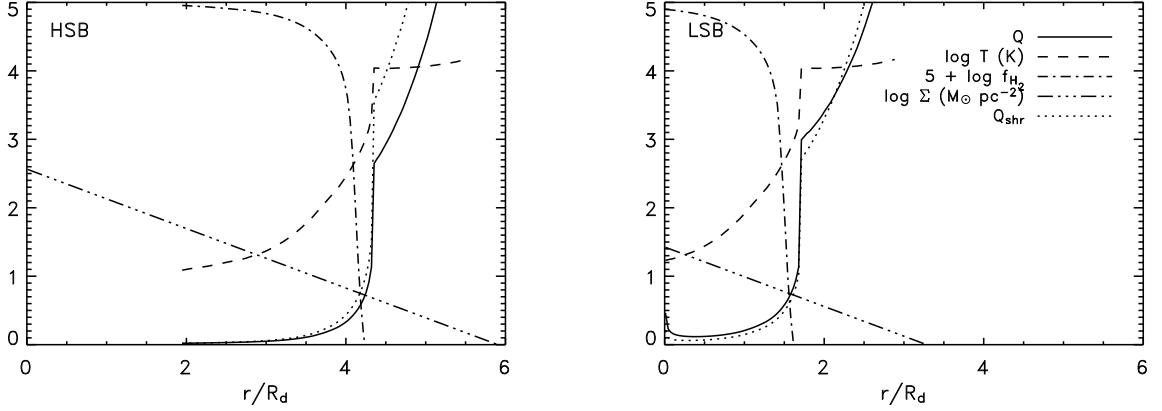
FIG. 2.— The Toomre Q parameter (*solid curves*), the temperature $\log T$ (*dashed curves*), the molecular fraction $5 + \log f_{H_2}$ (*dot-dashed* curves), the surface density $\log \Sigma (M_\odot \, pc^{-2})$ (*triple-dot–dashed curves*), and the Q parameter for shearing pertubations (*dotted curve*) are all plotted as a function of radius for models HSB (*left*) and LSB (*right*). The sudden drop in the Q values coincides with (and is caused by) a similar drop in the temperature, and a sharp increase in the molecular fraction. The transition to the cold phase, which coincides with the onset of gravitational instability ($Q < 1$), occurs at a fixed surface density. Note that the models become unrealistic shortwards of the critical radius, where feedback from star formation will increase the UV field, the metallicity, and the turbulent pressure.
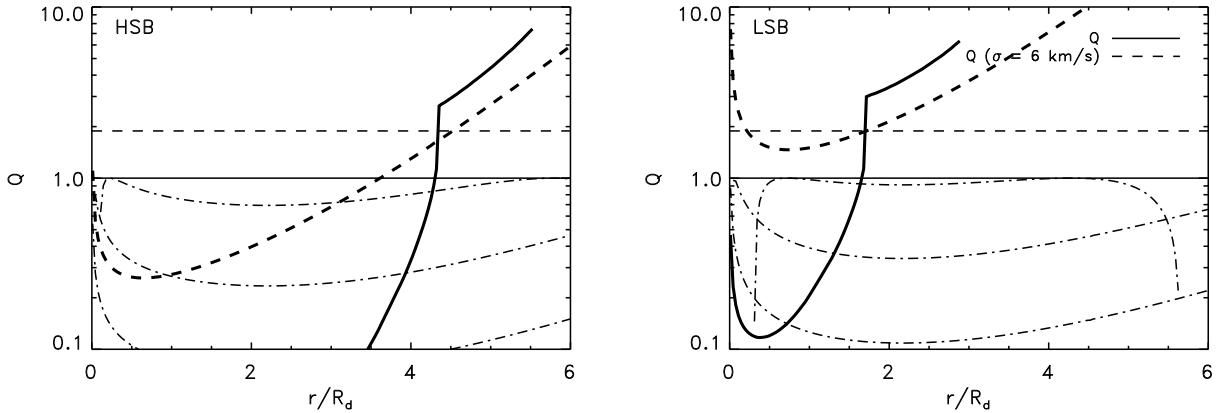

FIG. 3.— The Toomre Q parameter as a function of radius (*thick solid curves*) for models HSB (*left*) and LSB (*right*). The solid horizontal line indicates $Q = 1$. The sudden drop in the Q-value is caused by the transition to the cold phase. The dotted curves indicate the Q values below which the disk in unstable to perturbations with wavelengths of (*top*) 10^3, (*middle*) 10^2, and (*bottom*) 10 pc. Assuming a constant velocity dispersion of 6 km s^{-1} leads to large errors in the Q-parameter (*thick dashed curves*). The transition to the cold phase, which causes gravitational instability ($Q < 1$), occurs at about the radius where $Q(\sigma = 6 \, km \, s^{-1}) = 1/0.53$ (*intersection of thick dashed curves with horizontal dashed lines*), the empirical star formation threshold of MK01. This implies that the hypothesis that the star formation threshold is associated with the transition to the cold phase, is consistent with the observations. Note that the models become unrealistic shortwards of the critical radius, where feedback from star formation will increase the UV field, the metallicity, and the turbulent pressure.

Low surface brightness galaxies have lower surface densities, and therefore smaller optical radii (relative to their disk scale lengths). Note that in reality the situation could be more complicated if the values of the model parameters (f, Z, I) differ systematically between the outer disks of HSB and LSB galaxies.

Although the calculation of the radius within which the disk is unstable to star formation is robust, the detailed predictions of the models may be unrealistic for $r < r_c$. The model effectively predicts its own demise: within the critical radius feedback from star formation will modify the thermal and ionization structure of the disk and will generate turbulence, possibly leading to self-regulation of the SFR such that $Q \approx 1$. The energy injected by young stars and supernovae will also convert gas from the cold phase into the warm and/or a third (hot)

phase, and may introduce large fluctuations in the UV radiation. The models presented here may therefore be inadequate for studying star formation in the multiphase ISM. However, we emphasize that the prediction of widespread star formation at $r < r_c$ is robust, since the conditions that invalidate the model are *consequences* of this prediction.

It should, however, be noted that there are physical processes that have not been included in the models, which could result in the formation of high column density clouds in an otherwise warm phase. Examples are swing-amplifier instabilities, gravity-driven turbulence, infalling gas clouds, and spiral density waves. However, to form stars a cold phase is still required and consequently regions unstable to star formation should still have surface densities that exceed the threshold value. Hence, the local surface density threshold for star

formation would remain unchanged, but the conclusion that the phase transition triggers gravitational instability may no longer be correct, except for small-scale perturbations. Regardless of what comes first, such processes break the axisymmetry that was assumed in the models, and will thus break the one-to-one relationship between surface density and radius. This would complicate the interpretation of azimuthally smoothed observations, but it would not be in conflict with our criterion for star formation, which is a local threshold.

4.1. *The effects of turbulence*

Turbulence both prevents and promotes gravitational instability. It inhibits global collapse because it provides an additional source of pressure, but it can trigger local instability by creating density fluctuations. We will discuss each of these effects in turn.

Since the warm phase is gravitationally stable even in the absence of turbulence, increasing the amount of turbulent support will not change the conclusion that the presence of a cold phase is necessary for small-scale gravitational instability. However, if the turbulence is sufficiently strong, the presence of a cold phase may no longer be sufficient for instability. Turbulent support affects the Q parameter at the phase transition in two opposing ways. First, turbulent pressure increases the stability of the disk, approximately as[5] $Q \propto f_{th}^{-0.5}$ (recall that $f_{th} \equiv P_{th}/P \propto \sigma_{th}^2/\sigma^2$). Second, it increases the critical surface density for the transition to the cold phase (because it decreases the equilibrium density corresponding to a fixed surface density; see eq. [19]), which leads to a decrease in the Q parameter at the phase transition. In the next section we will show that this critical surface density scales approximately as $\Sigma_{\rm crit} \propto f_{th}^{-0.3}$. Thus, increasing the turbulence shifts the phase transition to higher surface densities (i.e., smaller radii) and increases the Q-value at this radius, approximately as $Q \propto f_{th}^{-0.5} f_{th}^{0.3} = f_{th}^{-0.2}$. Given that Q is very small within the critical radius for $f_{th} = 1$ (see, e.g., Fig. 2), it is clear that extremely large turbulent pressures are required to shift the instability to radii smaller than the radius of the phase transition.

Indeed, in our models the phase transition triggers instability for values of f_{th} as low as $1/250$, which corresponds to a line of sight velocity dispersion of $10(T/10^2 \ {\rm K})^{0.5} \ {\rm km \, s^{-1}}$ (for model LSB the derived critical surface densities exceed the central surface density if $f_{th} \ll 10^{-1}$). Higher turbulent pressures are ruled out as they would result in line of sight velocity dispersions that are significantly greater than the $8 \ {\rm km \, s^{-1}}$ that is typical for the extended H I disks of galaxies (e.g., Lo et al. 1993; Meurer et al. 1996).

Since turbulence locally compresses gas it can also induce instability. If the compression is sufficiently strong and happens on a timescale short compared with the cooling time, then the compressed gas could become gravitationally unstable while it is still in the warm phase. This situation is common in the multiphase ISM, where feedback from star formation is known to generate supersonic turbulence. As long as the turbulence is generated by feedback from star formation, we can ignore it for our purposes because we are only concerned with the validity of the models in the absence of star formation. There are, however, other processes capable of generating turbulence, such as swing-amplifier instabilities, shocks from spiral density waves, and infalling gas clouds.

---

[5] This scaling is only correct if magnetic pressure is negligible.
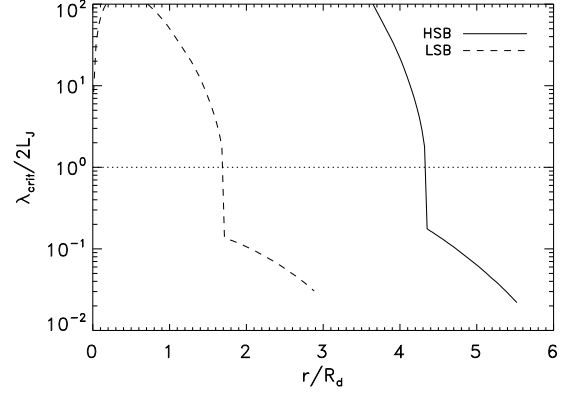

FIG. 4.— The ratio of the most unstable wavelength $\lambda_{\rm crit}/2$ (unstable for $Q < 1$) relative to the disk thickness ($\sim L_J$) as a function of radius. Longward of the critical radius for star formation, $\lambda_{\rm crit}$ is much smaller than the disk thickness, thereby invalidating the assumption that the disk is thin.

Although turbulence likely plays a central role in the multiphase ISM, there is in fact very little room for turbulence in the outer disk, because thermal motions in the gas heated by (extragalactic) UV radiation can by itself account for the observed widths of the H I lines. Indeed, proposed sources of turbulence in the extended gas disk appear unable to account for the observed velocity dispersion. Sellwood & Balbus (1999) estimate that MHD turbulence may result in a turbulent velocity dispersion of $6 \ {\rm km \, s^{-1}}$ (depending on the unknown strength of the magnetic field) and simulations by Wada, Meurer, & Norman (2002) show that gravity driven turbulence yields a velocity dispersion of only $2 - 3 \ {\rm km \, s^{-1}}$ in the outer disk. Thus, it appears likely that the turbulence in the extended gas disk, where there is no feedback from star formation, is mostly subsonic.

4.2. *On the applicability of the Toomre criterion*

In this section we further diminish the role of the Toomre criterion for star formation in the outer parts of galaxies by showing that it is not applicable to the warm extended gas disk and that it reduces to the Jeans criterion for the cold phase.

From equation (19) it can be seen that the disk thickness is about,

$$L_J \sim 4.4 \ {\rm kpc} \left(\frac{N_H}{10^{20.75}} \right)^{-1} f T_4. \qquad (22)$$

Thus, the transition from the cold to the warm phase results in a large increase in the disk scale height, and the disk is predicted to flare beyond the critical radius. However, in reality the flaring may be much less pronounced than predicted by equation (22) because the increase in T will be partially offset by a decrease in f_g (and thus f), because the effect of the dark halo may not be negligible for the warm, outer disk (e.g., Maloney 1993; Olling 1995). Moreover, if star formation is indeed ubiquitous when a cold phase is present, then the resulting turbulent pressure would decrease f_{th} (and thus increase f) within the critical radius.

Figure 4 demonstrates that the Toomre analysis is invalid for the warm, outer disk because the assumption that the disk is thin breaks down. The figure shows the ratio of the most unstable wavelength $\lambda_{\rm crit}/2$ (i.e., the wavelength of perturbations for which $Q_c = 1$; see eq. [8]) to the disk thickness L_J

(assuming $f = 1$), as a function of radius. Outside the critical radius the ratio $\lambda_{\rm crit}/2L_J$ is much smaller than unity, implying that the disk cannot be considered to be thin when investigating the stability of perturbations of size $\lambda \sim \lambda_{\rm crit}/2$. Since a thick disk is more stable than a thin disk (Romeo 1992), this reinforces the conclusion that the warm phase is gravitationally stable. The transition to the cold phase results in a large decrease in the disk scale height, and the assumption that the disk is thin does hold shortwards of the critical radius ($\lambda_{\rm crit}$ depends only on Σ and κ [see eq. [7]] and therefore varies smoothly across the critical radius).

The assumption that the disk is thin always becomes invalid for sufficiently small wavelengths. Figure 3 shows that the phase transition triggers instability on a large range of length scales. For perturbations with $\lambda \ll \lambda_{\rm crit}$, rotation is unimportant, and the Toomre criterion is equivalent to the Jeans criterion (see §2). Note, however, that since $L_J \sim 10^2$ pc in the cold phase (eq. [22]), the assumption that the disk is thin is only marginally valid for the smallest wavelengths that are predicted to be unstable.

Thus, for models HSB and LSB rotation has no effect on the star formation threshold in the outer disk. However, since the epicycle frequency diverges at $r = 0$, rotation will formally always stabilize the innermost parts of the disk. For example, rotation is responsible for the upturn in the Q parameter at $r < 0.3R_d$ that can be seen in figures 2 and 3 for model LSB. This effect is a direct consequence of the assumption that the galaxy can be described by a thin exponential disk all the way to $r = 0$. In reality this assumption breaks down and the epicycle frequency does not diverge. We have checked a wide variety of galaxy models and find that rotation can only stabilize the cold phase in the innermost part of the disk, $r \ll R_d$, where the epicycle frequency starts to diverge. The model predictions for the critical radius are therefore robust as long as $r_c \gtrsim R_d$, as is the case for observed disk galaxies. Note, however, that if one is interested in galaxies that are close to being completely dark [$\Sigma(r = 0) \approx \Sigma_{\rm crit}$], then any model that is based on a thin, exponential disk will give misleading results.

5. STAR FORMATION RECIPES

The critical surface density or, equivalently, the critical pressure above which a cold phase exists, depends on the factor f ($f \equiv f_g/f_{th}$, where f_g is the mass fraction in gas and f_{th} is the ratio of the thermal to total pressure), the metallicity Z, the intensity of the UV radiation I, and the dust-to-metals ratio. Because the critical radius for star formation in the outer disk is set by the transition to the cold phase, the star formation threshold is insensitive to the rotation curve of the galaxy. In this section we will present scaling relations for the critical surface density for star formation, which can be used in (semi-)analytic models of galaxy formation and evolution. Finally, we will present critical *volume* densities, which can be used to implement star formation thresholds in hydrodynamical simulations.

The sign of the dependence of the critical surface density on the various parameters is easy to predict: the phase transition occurs at a higher column density if the fraction of the mass in a collisionless component is lower (f_g higher), if the non-thermal pressure is higher (f_{th} lower), if the metallicity and dust content are lower (Z lower), and if the UV radiation is more intense (I higher). The exact scaling relations are, however, difficult to compute analytically. We will therefore simply provide fits to the results of our numerical calculations.

The following empirical formula provides a satisfactory fit to the column density at which the temperature is 500 K,

$$\log N_H(T = 500\,{\rm K}) \approx 20.75 \qquad (23)$$
$$+0.29\log(f) + 0.0052\log^2(f)$$
$$-0.32\log(Z/0.1Z_\odot) - 0.047\log^2(Z/0.1Z_\odot)$$
$$+0.23\log(I/10^6\,{\rm cm}^{-2}\,{\rm s}^{-1}) + 0.027\log^2(I/10^6\,{\rm cm}^{-2}\,{\rm s}^{-1}).$$

The column density for which the molecular fraction reaches one part in a thousand is fit well by the following formula,

$$\log N_H(f_{H_2} = 10^{-3}) \approx 20.75 \qquad (24)$$
$$+0.31\log(f) + 0.0025\log^2(f)$$
$$-0.32\log(Z/0.1Z_\odot) - 0.051\log^2(Z/0.1Z_\odot)$$
$$+0.26\log(I/10^6\,{\rm cm}^{-2}\,{\rm s}^{-1}) + 0.025\log^2(I/10^6\,{\rm cm}^{-2}\,{\rm s}^{-1}).$$

Finally, the following formula provides a good fit to the minimum column density for which the Toomre parameter equals unity

$$\log N_H(Q = 1) \approx 20.68 \qquad (25)$$
$$+0.28\log(f_g) + 0.020\log^2(f_g)$$
$$-0.35\log(f_{th}) + 0.030\log^2(f_{th})$$
$$-0.30\log(Z/0.1Z_\odot) - 0.047\log^2(Z/0.1Z_\odot)$$
$$+0.22\log(I/10^6\,{\rm cm}^{-2}\,{\rm s}^{-1}) + 0.041\log^2(I/10^6\,{\rm cm}^{-2}\,{\rm s}^{-1}).$$

The formulas given above can be used to implement star formation thresholds in (semi-)analytic models of galaxy formation and evolution. The fits were determined by running the model described in §3 for varying values of the parameters f_g, f_{th}, Z, and I. Each parameter was first varied separately, then the fits were optimized by varying multiple parameters simultaneously. Tests show that the errors in the fits to the predicted critical column densities are smaller than 0.25 dex over (at least) the range $f = 10^{-3} - 10^2$, $Z = 10^{-4} - 10\,Z_\odot$, and $I = 10^4 - 10^8$ photons cm^{-2} s^{-1}, with the exception of $N_H(T = 500\,{\rm K})$, which can be significantly in error for $Z \gtrsim 3Z_\odot$ because the large metal abundance causes the gas to cool below 500 K before the molecular fraction reaches 10^{-3} and the disk becomes unstable.

Although the above formulas fit the results of the models to within 0.25 dex, the systematic errors caused by the limitations of the model may be somewhat larger than 0.25 dex. In particular, our simplified prescription for hydrostatic equilibrium (see §3.1), cannot be expected to predict the critical surface densities with an accuracy better than a factor of a few. For example, the Jeans length is often defined with a factor of $\sqrt{\pi}$ that was not included in equation (19). The effect of including this factor is equivalent to setting $f_g = \pi$; i.e., the normalization of the three critical surface densities would be increased by about 0.15 dex.

Note that $N_H(Q = 1)$ depends explicitly on f_{th} because the Q parameter depends directly on the turbulent velocity dispersion. However, $N_H(Q = 1)$ scales with f_{th} in roughly the same way as $N_H(T = 500\,{\rm K})$ and $N_H(f_{H_2} = 10^{-3})$. Because the drop in the thermal velocity dispersion is large compared with the variation in the epicycle frequency at the phase transition, $N_H(Q = 1)$ is very insensitive to κ. We have tested a wide variety of galaxy models[6] and find that equation (25) works as

---

[6] The following parameter ranges were tested: $\lambda_{jd}/m_d = 0.01 - 0.3$, $c = 1 - 100$, $m_d = 0.005 - 1.0$, $M_{200} = 10^9$ to $5 \times 10^{13}\,{\rm M}_\odot$.

long as $r_c \gtrsim R_d$. As discussed in §4.2, for $r \ll R_d$ the epicycle frequency diverges and the innermost parts of disks are thus formally stabilized by rotation. However, for $r \ll R_d$ the scale height is no longer small compared to the radius and the Toomre criterion is not applicable. Furthermore, the centers of disk galaxies are generally dominated by a bulge component.

All three of the above formulas yield critical surface densities that depend only weakly on the values of the parameters f, Z, and I. Typically, a parameter has to change by a factor $\sim 10^3$ for the threshold surface density to change by a factor 10. The reason for this insensitivity to the values of the model parameters is hydrostatic equilibrium. For example, naively one might think that an increase of the UV radiation by a factor of 10 would result in a similar increase in the critical surface density. However, in hydrostatic equilibrium the volume density scales as the surface density squared (see eq. [19]) and because the cooling rate and the formation rate of molecular hydrogen increase with increasing density, the increase in the critical surface density is only about a factor of 2. It is important to note that if we had not assumed the disk to be self-gravitating (i.e., in approximate hydrostatic equilibrium), then agreement between the critical surface density and the observed star formation threshold would have required fine-tuning the parameters of the model.

The fact that equation (25) works for both models HSB and LSB, and that $N_H(Q = 1) \approx N_H(T = 500 \text{ K}) \approx N_H(f_{H_2} = 10^{-3})$ is consistent with the conclusion that the transition to the cold phase causes gravitational instability and that this transition coincides with a sharp increase in the molecular fraction (i.e., from $f_{H_2} \ll 10^{-3}$ to $f_{H_2} > 10^{-3}$). Using $T = 10^3$ K, or a molecular fraction smaller by one or two orders of magnitude gives almost identical results. The hydrogen column densities quoted above can be converted into surface densities using equation (20) and into pressures using equation (21). For example, the surface density and pressure corresponding to our fiducial threshold column density, $\log N_H = 20.75$ (in cm^{-2}), are $\log \Sigma = 0.77$ (M$_\odot$ pc^{-2}) and $\log P/k = 2.6$ (cm^{-3} K).

Although a critical column density is useful for (semi-)analytic work, it is of little use if only the volume density is known, as is generally the case for three-dimensional hydrodynamical simulations. Fortunately, assuming (approximate) hydrostatic equilibrium, the critical column density can be converted into a critical volume density using equation (19), provided that μ and T are known. For densities slightly below the threshold value, the gas will be warm and nearly fully atomic, and we can therefore assume $T \approx 10^4$ K and $\mu = 1/(1 - 3Y/4)$ (≈ 1.22 for $Y = 0.24$). Thus, a physically reasonable star formation recipe for a hydrodynamical simulation that lacks the physics needed to compute the transition to the cold phase self-consistently, is to convert gas elements with $T \sim 10^4$ K and density greater than a critical value computed from equation (19) and one of the fitting formulas above. For example, for our fiducial parameters ($f = 1$, $Z = 0.1Z_\odot$, $I = 10^6$ cm^{-2} s^{-1}) the critical density is $n_{H,\text{crit}} \approx 4 \times 10^{-2}$ cm^{-3}.

6. COMPARISON WITH OBSERVATIONS

In the previous sections it was argued that the transition to the cold phase leads to gravitational instability and star formation. This hypothesis leads to several predictions:

- Below the threshold surface density both the fraction of gas in the cold phase and the molecular fraction decline rapidly.

- The critical surface density depends (weakly) on the gas fraction, the amount of turbulence, the metallicity, and the intensity of the UV radiation. For reasonable parameter values the threshold surface density is $\Sigma_c \sim 3$–10 M$_\odot$ pc^{-2} ($N_{H,\text{crit}} \sim 3$–10×10^{20} cm^{-2}), which corresponds to a pressure $P/k \sim 10^2$–10^3 cm^{-3} K.

- Star formation thresholds are local: SF will occur wherever the gas surface density exceeds the local threshold value.

- If the disk has an exponentially declining surface density and is approximately axisymmetric, then the disk mass can be predicted if the critical radius r_c and the disk scale length R_d are measured.

In the remainder of this section we will discuss these predictions in detail and compare them with observations.

6.1. *Star formation thresholds*

Strong, direct evidence in favor of the hypothesis that the transition to the cold phase leads to star formation comes from high-resolution H I observations of 11 nearby spiral galaxies by Braun (1997). Braun found that the H I emission can be separated into two distinct components, associated with the cold and the warm phases respectively: (1) a high-brightness filamentary network that is marginally resolved at 150 pc and has a velocity FWHM less than 6 km s^{-1} and (2) a diffuse interarm and outer disk component. While the cold component accounts for 60%–90% of the line flux within the star forming disk, its contribution plummets abruptly near the edge of the optical disk.

Two further predictions of the model are that the critical surface density should be insensitive to the rotation curve and that the molecular fraction should rise sharply at the critical surface density. The fact that a fixed surface density threshold $\Sigma_g \sim 10$ M$_\odot$ pc^{-2} ($\log N_H \sim 21$) describes the observations reasonably well, has been known for some time (e.g., Skillman 1987; Taylor et al. 1994; Ferguson et al. 1998b; Lelièvre & Roy 2000) and the results of MK01 confirm this (see their Fig. 9, *bottom*). This critical value is close to the prediction for our fiducial parameter values: $\log N_{H,\text{crit}} \approx 20.75$. It is interesting to note that the observed scatter in $\Sigma_g(r_c)$ is smaller than the scatter in $Q(r_c)$ (compare Figs. 8 and 9, *bottom*, of MK01). Finally, MK01's figure 6 demonstrates that the molecular fraction indeed rises sharply at $\Sigma_g \sim 10$ M$_\odot$ pc^{-2} (see Wong & Blitz 2002 for additional evidence).

The sample of MK01 contains seven "subcritical" disks, i.e., galaxies for which $Q(\sigma = 6$ km s^{-1}) never reaches the critical value in the region of active star formation. However, inspection of their figure 5 (*bottom*) shows that all but one of these galaxies have $\Sigma_g \sim 10$ M$_\odot$ pc^{-2} for $r < r_c$. The one exception is NGC 4698, which is thought to have had its gas removed in a recent collision with another galaxy (Valluri & Jog 1990). Examples of disks with widespread star formation that are subcritical according to the K89 criterion, but which have $\Sigma \gtrsim 10$ M$_\odot$ pc^{-2}, have also been found in other studies (e.g., Thornley & Wilson 1995; Wong & Blitz 2002). Thus, observations indicate that a constant critical surface density works even when the K89 criterion fails.

Although the critical surface density predicted by the models for the fiducial parameter values is close to the observed value, the difference would have been somewhat greater if we

had used a radiation field with an intensity as small as expected for a purely extragalactic background. In §5 it was shown that using the extragalactic value ($\log I \sim 4.5$ photons cm^{-2} s^{-1}) instead of our fiducial value ($\log I = 6$), would yield a critical column density that is about a factor of two lower: $\log N_{H,\mathrm{crit}} \approx 20.4$. On the other hand, if we had allowed for some turbulence, the agreement would have improved. For example, using $f_{th} = 0.1$ (note that the total velocity dispersion is $\sigma \approx 9$ km s^{-1} $\sqrt{T_4/f_{th}}$) would increase the critical column density by about a factor of 2. The bottom line is that because of uncertainties in the model parameters, as well as systematic errors due to the limitations of the model, the predictions for the critical surface density are only accurate to within a factor of a few.

At present it is not even clear whether a threshold surface density of $\log N_{H,\mathrm{crit}} \approx 20.4$ is ruled out by the observations. The reason is that the value of 10 M$_\odot$ pc^{-2} is derived from azimuthally averaged observations. Ferguson et al. (1998b; see their Fig. 2) found that although the azimuthally averaged critical value is of order 10 M$_\odot$ pc^{-2}, individual H II regions have surface densities as low as 2 to 4 M$_\odot$ pc^{-2} ($\log N_H \approx 20.3$ - 20.6). The reason for the difference between local thresholds and the thresholds derived from azimuthally averaged observations could be spiral structure: if one defines the critical radius as the radius within which SF is ubiquitous, i.e., not confined to the spiral arms, then the interarm surface density will be near the threshold value, but the azimuthally averaged surface density will be larger.

Note that it does not make sense to measure the critical surface density without specifying the smoothing scale. After the surface density increases beyond the threshold value, the gas will fragment and the surface density of the individual clouds could become very large. The smoothing scale relevant for testing global star formation thresholds is probably similar to the size of H II regions.

It is interesting to compare the predicted critical column density for the phase transition with UV absorption line studies, which find that the transition occurs at $\log N_H \approx 20.3$–20.8 in the Galaxy (Savage et al. 1977) and at $\log N_H \approx 20.7$–21.2 in the Large Magellanic Cloud (Tumlinson et al. 2002). Using solar metallicity for the Galaxy, equation (25) predicts $\log N_{H,\mathrm{crit}} \approx 20.5$, in excellent agreement with the observations. Using a metallicity $Z = 0.2 Z_\odot$ for the LMC (e.g., Welty et al. 1999), we predict $\log N_{H,\mathrm{crit}} \approx 20.7$, which agrees with the lower range of the observed values. Since the LMC is actively forming stars, higher values of f and/or I may be more appropriate, in which case the predicted critical column density would be somewhat higher.

If gravitational instability is triggered by the drop in the velocity dispersion associated with the transition to the cold phase, then one would expect the function $Q(r)$ to be very different depending on whether the velocity dispersion is assumed to be constant, as is usually done in observational studies, or not. One may therefore reasonably ask why the Toomre criterion, combined with the assumption of a fixed velocity dispersion, has been reasonably successful in predicting the critical radius for star formation in spiral galaxies (e.g., K89; MK01).

Figure 3 shows a comparison of the real Q parameters (*thick solid curves*) and those computed under the assumption that $\sigma = 6$ km s^{-1} (*thick dashed curves*). Indeed, it is clear that the latter assumption leads to large errors in the Q parameter. The difference is particularly large for model LSB, whose entire disk is predicted to be stable if $\sigma = 6$ km s^{-1}. Hence, unless the velocity dispersion is set to the value appropriate for the transition to the cold phase ($T \sim 10^3$ K, $\sigma \approx 3$ km s^{-1}), assuming a constant velocity dispersion will yield a critical Toomre parameter different from unity.

Indeed, MK01, who carried out a thorough study of star formation thresholds in disk galaxies assuming $\sigma = 6$ km s^{-1}, found that the Toomre criterion only works if one takes $Q \approx 2.0$ as the critical value. Figure 3 shows that for both models HSB and LSB the critical radius, i.e., the radius for which $Q = 1$ (*intersection of thick solid curve with solid line*), is almost identical to the radius at which $Q(\sigma = 6$ km s$^{-1}) = 2$ (*intersection of thick dashed curve with horizontal dashed line*). This remarkable agreement shows that the model predictions are consistent with the empirical relation of MK01. Furthermore, because the difference in the assumed velocity dispersion can account for the claimed difference between the critical Q values for irregular (HEB98; Hunter et al. 2001) and spiral galaxies (K89; MK01), as discussed in §1, the model predictions also agree with observations of irregular galaxies.

In short, observations support the hypothesis that the transition to the cold phase determines the critical surface density, and that rotation has little effect on the star formation threshold in the outer parts of galaxies.

6.2. *Beyond the critical radius*

Since the star formation threshold in the outer disk is insensitive to the rotation rate, it is essentially a local criterion. Star formation will only cut off at the same radius throughout the disk if the surface density and the parameters f, Z, and I are axisymmetric. In particular, beyond the truncation radius of the stellar disk (i.e., the radius at which the azimuthally smoothed stellar surface density decreases sharply), star formation will occur wherever the local gas surface density exceeds the local threshold value. Observations of sporadic H II regions beyond the optical radius (e.g., Ferguson et al. 1998b; Brand et al. 2001) confirm that star formation thresholds are a local phenomenon (see also Skillman 1987; Hunter & Plummer 1996; HEB98; van Zee et al. 1997).

LSB galaxies have low star formation efficiencies despite the fact that their total gas content is normal. In LSB galaxies the gas is spread out over a larger area than in HSB galaxies, and consequently the surface density is lower (e.g., van der Hulst et al. 1993; van Zee et al. 1997). In our model the star formation threshold is generally not affected by the rotation rate, and the low rates of star formation in LSB galaxies and in the far outer parts of HSB galaxies have the same physical cause: the star formation efficiency is low because the azimuthally averaged gas surface density is below the threshold value. Although star formation is suppressed on average, local peaks in the gas surface density can still give rise to star formation, in agreement with observations (e.g., van Zee et al. 1997; HEB98). We note that this explanation also holds in the context of other interpretations of the star formation threshold (e.g., van der Hulst et al. 1993; Elmegreen & Parravano 1994).

For many spiral galaxies the truncation of the optical disk is known to be accompanied by a flaring of the H I disk (e.g., Bottema, Shostak, & van der Kruit 1987; Kamphuis & Briggs 1992). Our model can naturally account for the flaring of the gas disk beyond the truncation radius. The truncation of the stellar disk is caused by the star formation threshold which, in turn, arises due to the transition to the cold phase at the critical radius. The disk thickness is proportional to the temperature (see eq. [22]), which is predicted to increase sharply from $T <$

10^3 K at $r < r_c$ to $T \sim 10^4$ K at $r > r_c$. Hence, naively we would expect the disk thickness to increase abruptly from $\lesssim 10^2$ pc to $\gtrsim 1$ kpc at the edge of the stellar disk. In reality the increase in the disk scale height will be much smaller and more gradual than the increase in the temperature because the warm gas just beyond the threshold feels the full gravity of the neighboring cold gas and stars, and because the contribution of the dark halo may no longer be negligible compared to the self-gravity of the disk (i.e., the warm gas has effectively a low value of f). Moreover, within the critical radius turbulent pressure may increase the disk thickness (i.e., the cold gas may have a high value of f).

The flaring H I layer often exhibits a warp beyond the stellar disk (e.g., Briggs 1990) and for some galaxies, notably NGC 4013, the rotation curve exhibits a drop of as much as 10%–15% at the edge of the stellar disk (e.g., Bottema et al. 1987; Bottema 1996; van der Kruit 2001). It has been suggested (e.g., Florido et al. 2001) that the small, relatively sudden drop in the rotation curve at the optical edge of NGC 4013 poses a problem for theories that try to explain the observed cut-off in the SFR in terms of a surface density threshold. However, both observations (Swaters et al. 1997; Schaap, Sancisi, & Swaters 2000) and numerical models (Struck & Smith 1999) indicate that at large scale heights the gas rotates more slowly. Thus, it seems plausible that the small drop in the rotation curve of NGC 4013 is related to the flaring/warping of the disk (NGC 4013 has a strong warp). If, as suggested by Swaters et al. (1997), the decrease in the circular velocity with scale height is related to angular momentum conservation, then the effect on the rotation curve would be minimal if $r^2 \gg L^2$, where L is the disk thickness. It is therefore interesting that NGC 4013 has a smaller truncation radius ($r_c = 9.3$ kpc; Bottema 1996) than any of the 31 galaxies studied by Pohlen et al. (2000a, 2000b).

6.3. Disk sizes and masses

Observations indicate that stellar disks end rather abruptly (e.g., van der Kruit 1979; van der Kruit & Searle 1981; Barteldrees & Dettmar 1994; Fry et al. 1999; Pohlen et al. 2000a, 2000b; de Grijs, Kregel & Wesson 2001; Florido et al. 2001; Kregel, van der Kruit, & de Grijs 2002), although the sharpness of the truncation is still debated (e.g., Pohlen et al. 2002). Van der Kruit & Searle (1981) measured the truncation radius for a sample of 7 edge-on spirals and found that it occurs at a radius of 4.2 ± 0.5 exponential scale lengths (R_d) of the surface brightness distribution. More recently, Pohlen et al. (2000a) analyzed a sample of 31 nearby edge-on spiral galaxies and found $r_c/R_d = 2.9 \pm 0.7$, significantly lower than the value reported by van der Kruit & Searle (1981). The Pohlen et al. (2000a) sample is large enough to look for correlations between r_c and other parameters. Although Pohlen et al. (2000a) did not find a correlation between r_c/R_d and Hubble type, they did find an anti-correlation with R_d: large disks have relatively shorter cut-off radii. This anti-correlation can probably account for the differences between the results of van der Kruit & Searle (1981) and Pohlen et al. (2000a), as the sample of the latter authors contains more galaxies with large scale lengths.

If the critical radius for star formation remains fixed over a substantial part of the star formation history of the galaxy, then the star formation threshold will create a cut-off in the stellar surface density. The optical edge will in that case roughly coincide with the critical radius, provided that the galaxy formed inside-out.
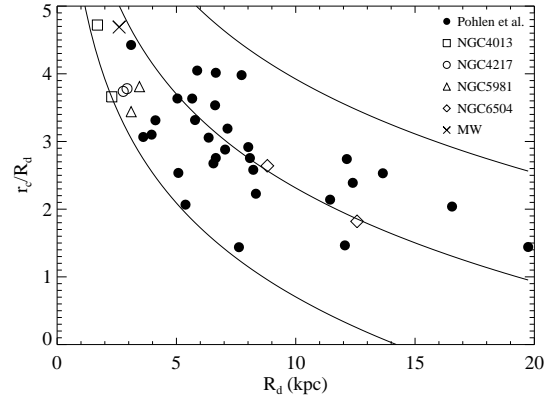

FIG. 5.— Disk size relative to disk scale length as a function of disk scale length, showing the sample of edge-on galaxies of Pohlen et al. (2000b; *solid points*), data taken from Florido et al. (2001; *open symbols*; there is one data point for either side of the galaxy), data for the Galaxy from Freudenreich (1998; *cross*), and the model predictions for $\log N_{H,\mathrm{crit}} = 20.75$ (*solid curves*) and $M_d/7.5 \times 10^9$ $M_\odot = 1$ (*top*), 5 (*middle*), and 25 (*bottom*). The models can clearly fit the observations for a reasonable range of disk masses.

From equation (15) it can be seen that for the MMW98 disk model the critical radius is given by

$$\frac{r_c}{R_d} = \ln \frac{m_d M_{200}}{2\pi\Sigma_c} - 2\ln R_d. \qquad (26)$$

The critical radius depends on the critical surface density Σ_c, the disk mass $m_d M_{200}$, and the disk scale length R_d. Note that there is a degeneracy in the models between increases in the critical surface density and decreases in the disk mass. If the ratio $m_d M_{200}/\Sigma_c$ is fixed, then r_c/R_d is anti-correlated with R_d.

Figure 5 (*filled circles*) shows the observations of Pohlen et al. (2000b). The anti-correlation between r_c/R_d and R_d reported by Pohlen et al. (2000a) is clearly visible[7]. The solid curves are the predictions of our model for our fiducial value of $\log N_{H,\mathrm{crit}} = 20.75$ ($\log \Sigma_c \approx 0.77$ $M_\odot$ pc^{-2}) and, from top to bottom, disk masses of 1, 5, and 25 times 7.5×10^9 $M_\odot$, respectively. The models can clearly reproduce the observed scaling of the size of the optical disk with the exponential scale length.

Figure 5 (*open symbols*) shows the results of Florido et al. (2001), who observed four edge-on spiral galaxies in the near infrared. Florido et al. measured the truncation radius and the disk scale length separately for each side of the galaxies, and hence there are two data points per galaxy in figure 5. While the two sides of the galaxies NGC 4217 and NGC 5981 give almost identical results, there are significant differences between the two sides for NGC 4013 and NGC 6504. What is interesting is that even though the two sides fall in different parts of the r_c/R_d-R_d diagram, they can both be fitted by a model with the same disk mass.

If the critical radius r_c and the disk scale length R_d have both been measured, then equation (26) can be used to predict the corresponding disk mass, which is proportional to

---

[7] Although the observed anti-correlation between r_c/R_d and R_d is suggestive, it should be kept in mind that it could be the result of measurement errors in R_d. Since disks are generally only well described by purely exponential profiles over at most a few scale lengths, and since the truncation radius is often not well defined, the measured values of R_d will depend somewhat on the definition of r_c (e.g., Pohlen 2001).

the assumed critical surface density Σ_c. Thus, if an independent estimate of the disk mass is available, then this provides an additional test of the model. For the Milky Way robust estimates of all three quantities have been published. Figure 5 (*cross*) shows the measurements of Freudenreich (1998): $R_d \approx 2.6$ kpc and $r_c/R_d \approx 4.7$. Equation (26) then yields a disk mass $M_d \approx 2.7 \times 10^{10}$ M$_\odot$, remarkably close to the results of Dehnen & Binney (1998), who found $M_d = 3$–5×10^{10} M$_\odot$ from various observational constraints.

A consistency check is possible even if no measurements of the disk mass are available: we can compute the mass-to-light ratio of the disk and compare it with expectations from population synthesis models. The total mass-to-light ratio of the disk in the X band, Υ_X, is given by

$$2.5\log\Upsilon_X = M_X - M_X(\odot) + 2.5\log M_d/M_\odot, \qquad (27)$$

where M_X and $M_X(\odot)$ are the absolute magnitudes of the galaxy and the sun respectively. Population synthesis models yield *stellar* mass-to-light ratios, whereas the above equation predicts the *total* mass-to-light ratio. While the surface density of the disk is generally dominated by stars in the inner parts of the galaxy, their contribution is very small for $r > r_c$. Since the fraction of the total disk mass exterior to r_c is not always negligible for an exponential disk, we need to use the disk mass interior to r_c, $M_d(r_c) = [1 - \exp(-r_c/R_d) - r_c/R_d \exp(-r_c/R_d)]M_d$, when computing Υ. This still gives only an upper limit to the stellar mass-to-light ratio, because it includes the mass in gas.

Figure 6 shows the resulting mass-to-light ratio in the B band for the sample of Pohlen et al. (2000b), computed using the distances listed by those authors, the apparent magnitudes from the NASA Extragalactic Database[8] (corrected for Galactic extinction using the results of Schlegel, Finkbeiner, & Davis 1998), and $M_B(\odot) = 5.48$. The mass-to-light ratios scatter between 1 and 5.5, with a mean of 3.1. Note that all points can be moved up and down in proportion to the critical surface density (we used our fiducial value $\log N_{H,\text{crit}} = 20.75$). The scatter may not be real, since there are (unknown) errors in the measurements of r_c, R_d, m_B, the distances, and of course in the model. Furthermore, there may be small differences in the real critical surface densities from one galaxy to the next, depending on the appropriate values of f, Z, and I. Nevertheless, the predicted values for the total mass-to-light ratio are in accord with the predictions of population synthesis models for the stellar mass-to-light ratio in the B band (e.g., Bell & de Jong 2001). Hence, we conclude that the model predicts disk masses that are consistent with the observations.

6.4. *Uncertainties*

Although the agreement between the model and observations is encouraging, it is important to keep in mind that there are considerable uncertainties in both the observational results and the theoretical predictions.

The observables required to test the Toomre criterion are the rotation curve, the surface densities in atomic and molecular gas, and the velocity dispersion. The latter two quantities are most difficult to measure with sufficient accuracy.

One important source of error for all observables is azimuthal smoothing. Azimuthal smoothing would be harmless if galaxies were perfectly axisymmetric, but the presence of spiral structure proves that they are not. Although the models are axisymmetric, the star formation threshold criterion does
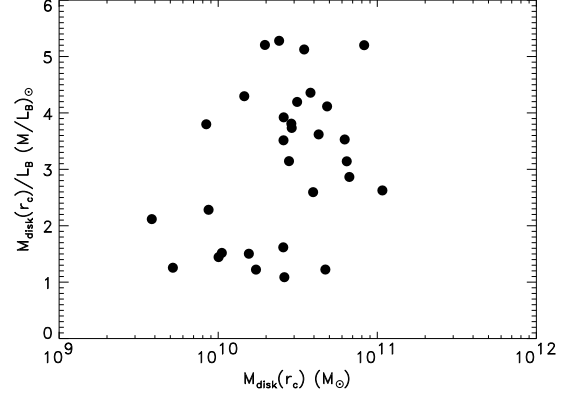
FIG. 6.— The predicted mass-to-light ratio in the B-band versus the predicted disk mass interior to the critical radius for the sample of Pohlen et al. (2000b). These mass-to-light ratios are based on the total disk mass and are thus upper limits for the stellar mass-to-light ratios. Disk masses are computed from the measured critical radii and disk scale lengths, and are proportional to the assumed critical surface density. The results fall within the range expected for B-band stellar mass-to-light ratios (e.g., Bell & de Jong 2001), indicating that the disk masses predicted by the model are consistent with the observations.

not require this. The fate of a perturbation, which does not have to be ringlike, depends on the local rotation rate and the local surface density. Hence, for non-axisymmetric galaxies the critical radius is not well defined, and individual regions beyond the azimuthally smoothed threshold can form stars if their surface density exceeds the local threshold value.

The molecular gas surface densities are derived from CO maps, using a conversion factor that has been calibrated using local, Galactic observations, i.e., using gas with a metallicity that may be considerably higher than in the outer disk. The CO maps rarely cover the outer parts of the disk and the H$_2$ column near the optical radius is therefore generally estimated by extrapolating the trend measured at smaller radii. If the models are correct, then the molecular fraction rises sharply shortwards of the critical radius (see Fig. 2), and extrapolating the H$_2$ surface density would result in an overestimate of the threshold surface density.

The velocity dispersion is very difficult to measure and is therefore usually assumed to be constant. To test whether, as argued here, the star formation threshold is set by the transition to the cold phase, one would like to measure the change in the velocity dispersion. However, even if one could measure the dispersion, the interpretation would not be straightforward because the ISM will be multiphase shortwards of the critical radius, whereas it is only the velocity dispersion of the cold phase that is relevant. More importantly, it is likely that there is no sharp decrease in the velocity dispersion because feedback from star formation will generate turbulence, which could lead to self-regulation (i.e., $Q \approx 1$). Note that this is fully consistent with the hypothesis that the transition to the cold phase is responsible for the observed cut-off in the star formation rate. All that this hypothesis requires, is that the velocity dispersion is small in the absence of star formation.

Of course, the model also suffers from uncertainties. Although the assumptions of plane-parallel radiative transfer, a step-function vertical density profile, thermal equilibrium, and hydrostatic equilibrium do capture most of the relevant physics, they are approximations. Note that the latter assump-

tion does not even hold exactly in our model: even though we compute physical quantities like the density, temperature and disk thickness as a function of radius, we ignore the effects of gradients in these quantities when doing so. Nevertheless, it is demonstrated in the appendix that the model accurately predicts the disk thickness of an isothermal, exponential disk. On the other hand, the rapid change in the temperature at the critical radius probably causes us to overestimate the sharpness of the decrease in the scale height (the thin, cold disk decreases the effective f-value for the neighboring warm, thick disk). Moreover, for the warm, outer disk the effect of the dark halo may no longer be negligible compared to the self-gravity of the disk (again, this would decrease the f-value for the warm disk). However, the phase transition should remain sharp, because the gas is thermally unstable at intermediate temperatures, and because self-shielding and the formation of molecular hydrogen provide positive feedback loops.

Our model does not include several physical processes that could in principle trigger star formation in the otherwise warm, outer disk. Examples are swing-amplifier instabilities and spiral density waves. If these processes are important, then they could undermine the conclusion that the phase transition triggers gravitational instability. However, to form a cold, molecular phase, regions of enhanced density will still have to exceed the critical surface density and the phase transition will still trigger instability on small scales. Although gravity-driven turbulence seems unavoidable, we note that recent simulations (e.g, Wada et al. 2002) indicate that in the extended disk, beyond the critical radius for star formation, the typical turbulent velocity dispersion is substantially below the typical observed value ($8\,\mathrm{km\,s^{-1}}$), which, in our model, corresponds to the thermal velocity dispersion of the warm phase.

Perhaps even more important than the uncertainties in the model assumptions are the uncertainties in the model parameters, in particular f, Z, and I. In §3.3 we motivated our fiducial values ($f = 1$, $Z = 0.1\,\mathrm{Z_\odot}$, $I = 10^6$ photons $\mathrm{cm^{-2}\,s^{-1}}$). In §5 it was shown that the critical surface density is fairly insensitive to the values of these parameters. Typically, a parameter has to change by a factor $\sim 10^3$ for the threshold surface density to change by a factor 10. Nevertheless, the large uncertainty in the appropriate values for the turbulent pressure and the intensity of the UV radiation imply that the predictions could be off by a factor of a few.

7. CONCLUSIONS

Observations indicate that disk galaxies have rather sharp edges: both the SFR and the stellar surface density decline sharply beyond a few disk scale lengths. These observations are usually explained in terms of a star formation threshold, set by the Toomre criterion for gravitational instability in a thin, rotating disk (e.g., Spitzer 1968; K89). Neither rotation nor pressure can stabilize the disk if the Toomre Q parameter ($Q \equiv c_s \kappa / \pi G \Sigma_g$) is smaller than unity or, equivalently, if the surface density exceeds the critical value $c_s \kappa / \pi G$. Since it is difficult to measure the velocity dispersion σ (and thus the sound speed c_s), observational studies usually assume a fixed value. Provided that the threshold Q value is allowed to differ from unity, and to be different for spirals and irregulars, the Toomre criterion appears reasonably successful. However, observations of "subcritical disks" (i.e., $Q > Q_c$ everywhere) with widespread star formation and of H II regions beyond the critical radius [$= r(Q = Q_c)$] have cast doubt on the general applicability of a Q threshold. As an alternative, Elmegreen & Parravano (1994) have emphasized that the need for a cold

phase to form stars introduces a minimum critical pressure, which depends on the radiation field and the metallicity. They argued that high Q values prevent star formation indirectly because they inhibit the formation of regions with sufficiently high pressures to contain a multiphase ISM.

To investigate the physical cause of the observed star formation threshold in the outer parts of galaxies, a model was constructed for a gaseous, exponential disk embedded in a dark halo. The disk is self-gravitating, contains metals and dust, and is illuminated by UV radiation. It was found that the critical surface density for the transition to the cold phase agrees with empirically derived constant star formation thresholds (e.g., Skillman 1987), which therefore supports the idea of Elmegreen & Parravano (1994) that a cold phase is critical to star formation (see also HEB98, Hunter et al. 2001, Billett et al. 2002, and Elmegreen 2002).

In the models the drop in the thermal velocity dispersion associated with the transition from the warm ($T \sim 10^4$ K) to the cold ($T < 10^3$ K) phase causes the disk to become gravitationally unstable on a large range of scales, which suggests that this phase transition plays a more important role than had hitherto been recognized. Since stars form in molecular clouds, it is likely that the presence of a cold, gravitationally unstable phase will lead to star formation. The transition to the cold phase is sharp because the gas is thermally unstable at intermediate temperatures and because both self-shielding and the formation of molecular hydrogen provide positive feedback loops. The phase transition is associated with a sharp increase in the molecular fraction (from $f_{H_2} \ll 10^{-3}$ to $f_{H_2} > 10^{-3}$), in agreement with observations.

Galactic rotation, which includes both the Coriolis force and shear, does not affect the critical surface density at which the phase transition occurs and cannot stabilize the cold phase in the outer disk. It is, however, important to note that insofar as the Toomre Q parameter controls the formation of global perturbations such as spiral arms and bars, it can have an indirect effect on the ability of the disk to form regions in which the surface density exceeds the threshold value for the transition to the cold phase (Elemgreen & Parravano 1994), which could then trigger gravitational instability on smaller scales.

While turbulence ultimately has a stabilizing effect, it can also promote local collapse by generating density enhancements. Turbulence driven by feedback from star formation should not be taken into account when computing a global star formation threshold. However, there exists several physical mechanisms that could drive turbulence even in the absence of star formation, but which were not included in the models. Examples are infalling gas clouds, shocks from spiral density waves, and the magnetorotational instability. We argued that it is unlikely that turbulence dominates the velocity dispersion of the gas in the extended H I disks, which can be accounted for entirely by thermal motions provided it is kept warm by the (extragalactic) UV radiation, as predicted by the model.

Although the presence of strong turbulent support would increase the critical surface density, it would not undermine the conclusion that the transition to the cold phase triggers instability. The reason is that turbulent support increases the surface density required for the phase transition by about as much as it increases the velocity dispersion of the gas, thereby leaving the Q parameter at the phase transition nearly unchanged. In the models the phase transition triggers instability for turbulent pressures as large as 250 times the thermal pressure. Such a high turbulent pressure would give rise to velocity dispersions that are ruled out by measurements of H I line widths

in the outer parts of galaxies.

Although the model used here can predict the threshold surface density above which some of the gas will become cold and unstable to fragmentation, it cannot predict which fragments will succeed in forming stars. Moreover, once stars form, feedback processes will create a complex, multiphase ISM that is not well described by the simple model. Hence, the predicted critical surface densities should be interpreted as global star formation thresholds.

The critical radius for star formation can be defined as the radius within which the azimuthally averaged surface density exceeds the critical value required for the transition to the cold phase (e.g., Elmegreen & Parravano 1994). However, since rotation is generally unimportant, star formation thresholds are a local phenomenon: peaks in the surface density that exceed the threshold value will form stars regardless of their position in the disk. Thus, sporadic star formation beyond r_c is possible, in particular in spiral arms (e.g., van Zee et al. 1997; HEB98). Compared to high surface brightness galaxies, low surface brightness galaxies have low star formation efficiencies because their (azimuthally averaged) surface density becomes subcritical at smaller radii relative to their disk scale length (e.g., van der Hulst et al. 1993).

The model can account for the radii and surface densities at which the SFR is observed to cut off. Model predictions regarding the scaling of the size of the stellar disk with the disk mass and scale length agree with the observations. In particular, the mass-to-light ratios predicted on the basis of measured values of the critical radius, the disk scale length, and the luminosity, are consistent with expectations from population synthesis models.

Scaling relations were computed for the dependence of the critical column density on the intensity of the UV-radiation, the metallicity, the relative importance of thermal and turbulent pressure, and the mass fraction in stars and dark matter. Assuming hydrostatic equilibrium, the critical column density can be converted into an equivalent critical pressure or volume density. These scaling relations can be used to implement star formation thresholds in (semi-)analytic models and three-dimensional hydrodynamical simulations of galaxy formation. For reasonable parameter values, we find a critical surface density $\Sigma_c \sim 3\text{–}10\ M_\odot\ \mathrm{pc}^{-2}$ ($N_{H,\mathrm{crit}} \sim 3\text{–}10 \times 10^{20}\ \mathrm{cm}^{-2}$), which corresponds to a pressure $P/k \sim 10^2\text{–}10^3\ \mathrm{cm}^{-3}\ \mathrm{K}$, and a volume density $n_H \sim 10^{-2}\text{–}10^{-1}\ \mathrm{cm}^{-3}$.

Thus, the hypothesis that the transition to the cold phase triggers gravitational instability and star formation, leads to a large number of predictions that appear to be supported by available observations. It provides an explanation for a range of observed phenomena and correlations, some of which were thought to be unrelated. Future observations, as well as numerical simulations that include radiative transfer, molecules, dust, and metals, could test these predictions in more detail and help refine the model.

APPENDIX

In this section it is demonstrated that for the case of a gaseous isothermal exponential disk, equation (19) is a very good approximation to the exact solution. The density profile for an isothermal exponential disk is,

$$\rho(r,z) = \frac{\Sigma(r)}{2H(r)} \mathrm{sech}^2 \left(\frac{z}{H(r)} \right), \tag{1}$$

where the scale height H is given by

$$H = \frac{c_s^2}{\pi G \Sigma} \tag{2}$$

(Spitzer 1942). For the purpose of the radiative transfer calculation, the characteristic density at radius r is the column density weighted density

$$\langle \rho \rangle_N \equiv \frac{1}{\Sigma} \int \rho^2 dz = \frac{\Sigma}{3H}. \tag{3}$$

Ignoring the small mass contained in metals, the total hydrogen column density $N_H = \Sigma(1-Y)/m_H$ can then be written as,

$$N_H = \left(\frac{3}{\pi} \right)^{1/2} \left(\frac{\gamma k}{\mu m_H^2 G} \right)^{1/2} (1-Y)^{1/2} n_H^{1/2} T^{1/2}, \tag{4}$$

where $n_H \equiv \langle \rho \rangle_N (1-Y)/m_H$ is the characteristic hydrogen number density. This expression differs from equation (A5) of Schaye (2001a; our eq. [19]), which was derived by equating the sound crossing time and the dynamical time, by a factor $\sqrt{3/\pi} \approx 0.98$.

REFERENCES

Barteldrees, A. & Dettmar, R.-J. 1994, A&AS, 103, 475
Bell, E. F. & de Jong, R. S. 2001, ApJ, 550, 212
Billett, O. H., Hunter, D. A., & Elmegreen, B. G. 2002, AJ, 123, 1454
Binney, J., & Tremaine, S. 1987, Galactic Dynamics (Princeton: Princeton Univ. Press)
Black, J. H. 1987, ASSL Vol. 134: Interstellar Processes, 731
Bland-Hawthorn, J. & Maloney, P. R. 1999, ASP Conf. Ser. 166: Stromlo Workshop on High-Velocity Clouds, 212
Bland-Hawthorn, J. & Maloney, P. R. 2002, ASP Conf. Ser. 254: Extragalactic Gas at Low Redshift, 267

Borriello, A. & Salucci, P. 2001, MNRAS, 323, 285
Bottema, R. 1996, A&A, 306, 345
Bottema, R., Shostak, G. S., & van der Kruit, P. C. 1987, Nature, 328, 401
Brand, J., Wouterloot, J. G. A., Rudolph, A. L., & de Geus, E. J. 2001, A&A, 377, 644
Braun, R. 1997, ApJ, 484, 637
Briggs, F. H. 1990, ApJ, 352, 15
Corbelli, E. & Salpeter, E. E. 1995, ApJ, 450, 32
Corbelli, E., Galli, D., & Palla, F. 1997, ApJ, 487, L53
de Grijs, R., Kregel, M., & Wesson, K. H. 2001, MNRAS, 324, 1074

Dehnen, W. & Binney, J. 1998, MNRAS, 294, 429

Elmegreen, B. G. 1993, in Star-Forming Galaxies and Their Interstellar Media, ed. J. Franco, F. Ferrini, & G. Tenorio-Tagle (Cambridge: Cambridge Univ. Press), 337

Elmegreen, B. G. 2002, ApJ, 577, 206

Elmegreen, B. G. & Parravano, A. 1994, ApJ, 435, L121

Fall, S. M. & Efstathiou, G. 1980, MNRAS, 193, 189

Ferguson, A. M. N., Gallagher, J. S., & Wyse, R. F. G. 1998a, AJ, 116, 673

Ferguson, A. M. N., Wyse, R. F. G., Gallagher, J. S., & Hunter, D. A. 1998b, ApJ, 506, L19

Ferland, G. J. 2000, Revista Mexicana de Astronomia y Astrofisica Conference Series, 9, 153

Ferland, G. J., Korista, K. T., Verner, D. A., Ferguson, J. W., Kingdon, J. B., & Verner, E. M. 1998, PASP, 110, 761

Field, G. B. 1965, ApJ, 142, 531

Florido, E., Battaner, E., Guijarro, A., Garzón, F., & Jiménez-Vicente, J. 2001, A&A, 378, 82

Freudenreich, H. T. 1998, ApJ, 492, 495

Fry, A. M., Morrison, H. L., Harding, P., & Boroson, T. A. 1999, AJ, 118, 1209

Gerritsen, J. P. E. & Icke, V. 1997, A&A, 325, 972

Goldreich, P. & Lynden-Bell, D. 1965, MNRAS, 130, 125

Haardt, F., & Madau, P. 2001, in 21st Moriond Astrophys. Meeting, Clusters of Galaxies and the High-Redshift Universe Observed in X-rays: Recent Results of *XMM-Newton* and *Chandra*, ed. D. M. Neumann & J. T. T. Van (Paris: Editions Frontieres)

Henry, R. B. C. & Worthey, G. 1999, PASP, 111, 919

Hunter, D. A. & Plummer, J. D. 1996, ApJ, 462, 732

Hunter, D. A., Elmegreen, B. G., & Baker, A. L. 1998, ApJ, 493, 595 (HEB98)

Hunter, D. A., Elmegreen, B. G., & van Woerden, H. 2001, ApJ, 556, 773

Kamphuis, J. & Briggs, F. 1992, A&A, 253, 335

Kennicutt, R. C. 1989, ApJ, 344, 685 (K89)

Kregel, M., van der Kruit, P. C., & de Grijs, R. 2002, MNRAS, 334, 646

Lelièvre, M., & Roy, J. 2000, AJ, 120, 1306

Lo, K. Y., Sargent, W. L. W., & Young, K. 1993, AJ, 106, 507

Maloney, P. 1993, ApJ, 414, 41

Martin, C. L. & Kennicutt, R. C. 2001, ApJ, 555, 301 (MK01)

Meurer, G. R., Carignan, C., Beaulieu, S. F., & Freeman, K. C. 1996, AJ, 111, 1551

Mo, H. J., Mao, S., & White, S. D. M. 1998, MNRAS, 295, 319 (MMW98)

Navarro, J. F., Frenk, C. S., & White, S. D. M. 1997, ApJ, 490, 493 (NFW)

Oh, S. P. & Haiman, Z. 2002, ApJ, 569, 558

Olling, R. P. 1995, AJ, 110, 591

Pettini, M., King, D. L., Smith, L. J., & Hunstead, R. W. 1997, ApJ, 478, 536

Pettini, M., Ellison, S. L., Steidel, C. C., & Bowen, D. V. 1999, ApJ, 510, 576

Pohlen, M. 2001, PhD Thesis, Ruhr-University Bochum, Germany

Pohlen, M., Dettmar, R.-J., & Lütticke, R. 2000a, A&A, 357, L1

Pohlen, M., Dettmar, R.-J., Lütticke, R., & Schwarzkopf, U. 2000b, A&AS, 144, 405

Pohlen, M., Dettmar, R.-J., Lütticke, R., & Aronica, G. 2002, A&A, 392, 807

Quirk, W. J. 1972, ApJ, 176, L9

Romeo, A. B. 1992, MNRAS, 256, 307

Safronov, V. S. 1960, Annales d'Astrophysique, 23, 979

Savage, B. D., Drake, J. F., Budich, W., & Bohlin, R. C. 1977, ApJ, 216, 291

Schaap, W. E., Sancisi, R., & Swaters, R. A. 2000, A&A, 356, L49

Schaye, J. 2001a, ApJ, 559, 507

Schaye, J. 2001b, ApJ, 562, L95

Schlegel, D. J., Finkbeiner, D. P., & Davis, M. 1998, ApJ, 500, 525

Scott, J., Bechtold, J., Morita, M., Dobrzycki, A., & Kulkarni, V. 2002, ApJ, 571, 665

Sellwood, J. A. & Balbus, S. A. 1999, ApJ, 511, 660

Skillman, E. D. 1987, in Star Formation in Galaxies, edited by C. J. Londsdale Persson (NASA Conf. Pub. CP-2466), p. 263

Spitzer, L. J. 1942, ApJ, 95, 329

Spitzer, L. 1968, Diffuse Matter in Space (New York: Wiley)

Struck, C. & Smith, D. C. 1999, ApJ, 527, 673

Swaters, R. A., Sancisi, R., & van der Hulst, J. M. 1997, ApJ, 491, 140

Taylor, C. L., Brinks, E., Pogge, R. W., & Skillman, E. D. 1994, AJ, 107, 971

Thornley, M. D. & Wilson, C. D. 1995, ApJ, 447, 616

Toomre, A. 1964, ApJ, 139, 1217

Tumlinson, J. et al. 2002, ApJ, 566, 857

Valluri, M. & Jog, C. J. 1990, ApJ, 357, 367

van den Bosch, F. C. & Swaters, R. A. 2001, MNRAS, 325, 1017

van der Hulst, J. M., Skillman, E. D., Smith, T. R., Bothun, G. D., McGaugh, S. S., & de Blok, W. J. G. 1993, AJ, 106, 548

van der Kruit, P. C. 1979, A&AS, 38, 15

van der Kruit, P. C. 1988, A&A, 192, 117

van der Kruit, P. C. 2001, ASP Conf. Ser. 230: Galaxy Disks and Disk Galaxies, 119

van der Kruit, P. C. & Searle, L. 1981, A&A, 95, 105

van Zee, L., Haynes, M. P., Salzer, J. J., & Broeils, A. H. 1997, AJ, 113, 1618

Vladilo, G. 1998, ApJ, 493, 583

Wada, K., Meurer, G., & Norman, C. A. 2002, ApJ, 577, 197

Welty, D. E., Frisch, P. C., Sonneborn, G., & York, D. G. 1999, ApJ, 512, 636

Wong, T. & Blitz, L. 2002, ApJ, 569, 157